ELSEVIER

Materials Science and Engineering B45 (1997) 152–161

MATERIALS SCIENCE & ENGINEERING B

Preferred orientations and epitaxial relationships of α-HgI_2 thin films on (001)-KCl and (001)-Muscovite single crystals

D. Chateigner [a,b,*], B. Erler [c,d]

[a] *Lab. de Cristallographie-CNRS, BP166 F-38042, Grenoble cedex 09, France*
[b] *Department of Geology and Geophysics, UC Berkeley, Berkeley, CA-94720, USA*
[c] *Lab. f. Festkörperphysik, ETH Hönggerberg, CH-8093 Zürich, Switzerland*
[d] *Kris. Inst., f. Universität Freiburg, D-79104 Freiburg, Germany*

Received 22 October 1996; accepted 10 November 1996

Abstract

The quantitative texture analysis of HgI_2 films deposited on KCl and Muscovite single crystal substrates is reported. The lattice parameters of the films have been refined. They are close to the bulk α-HgI_2 tetragonal structure. The films are strongly in-plane oriented. Complex pole figures are observed, explained after the orientation distribution calculation, using a direct method. Orientation maxima as high as 248 times the random distribution are observed for the orientation distribution, with texture index up to 44. The orientations are governed by heteroepitaxial relationships. Three relations are observed and described for each substrate, which are explained by close distance matching between the film and the substrate. Additional texture symmetry is provided by the substrate crystal-plane, four-fold in the case of KCl and six-fold for muscovite. © 1997 Elsevier Science S.A.

Keywords: Epitaxial relationships; Mercury iodide; Muscovite single crystals; Orientation distribution

1. Introduction

For many years gas proportional detectors or scintillators were the only ones used in diffraction experiments, mainly because of their earlier industrial development and practical use. Unfortunately the former generally have a poor resolution in energy, and cannot be employed when X-ray fluorescence occurs, except when the experimental setup is modified (by changing the incident X-ray radiation source, adding monochromators or electronic filtering for example). However, those modifications are often undesirable for practical purposes because they result in time consuming experiments and experimental complexity. Solid state detectors were developed later in order to solve some of the problems encountered with gas detectors. Moreover, they appeared to be powerful tools for collecting diffraction or fluorescence patterns on two dimensions, and are now widely used for Laüe or Debye-Scherrer imaging at most synchrotron radiation sources for example [1], because they furnish quantitative information whereas classical films saturate or have insufficient resolution.

Besides these advantages, one can hope to solve several problems, for instance laser strikes when reading overloaded image plates, by employing new materials and using new synthesis procedures. Among different materials known as potential X-ray detectors, mercury iodide seems promising because of its large bandgap extended to gamma ray capture range [2]. However, bulk HgI_2 crystals are subject to high mechanical sensitivity during manufacturing [3] which can result in low quality detectors [4]. Thin film deposition might play a key role here, enabling fabrication of larger and cheaper detectors in desired shapes.

Resulting from its crystalline structure and from substrate interactions, the growth of thin films is achieved with preferentially induced orientations, which one would expect to modify the required properties or film's stability and aging. Only a few works, to our knowledge, have been dedicated to the fabrication of oriented α-HgI_2 films, and to their characterization, though qualitatively [5]. In this study X-ray diffraction

* Corresponding author. Tel.: +33 476 887421; fax: +33 476 881038; e-mail: chateign@labs.polycnrs-gre.fr

PII S0921-5107(96)02035-1

quantitative texture analysis has been used in order to determine the growth relations existing between the α-HgI_2 films and two kinds of single crystal substrates, (001)-KCl and (001)-Muscovite.

2. Experimental

2.1. Film deposition

The optically active phase of mercury iodide for γ- or X-ray detectors is the α tetragonal form ($P4_2/nmc$, $a = 4.3693$ Å and $c = 12.4399$ Å) [6]. The orientation of its yellow orthorhombic modification, β-HgI_2, stable above 127°C, has been reported [7], but does not offer the researched properties.

The films were deposited using a sublimation process. Their growth took place in a furnace with two heater zones. Substrate and source were placed at the bottom and top of an ampoule respectively, air is evacuated and the ampoule sealed. Highly purified mercury iodide is used as the source material; the purification procedure has been described elsewhere [8]. Transport of the material from the source to the substrate took place due to the applied temperature gradient.

Four samples were studied by X-ray diffraction. Three of them (A, B and C) were deposited on the (001) plane of KCl single crystals (Fm3m, $a = 6.2917$ Å), while sample D was deposited on Muscovite 2N1 (C2/c, $a = 5.19$ Å, $b = 9.03$ Å, $c = 20.05$ Å, $b = 95.77°$). The film thickness in each case was 10 μm.

2.2. X-ray diffraction and texture analysis

X-ray diffraction and texture analysis experiments were performed using a Seifert high resolution texture goniometer in the Schulz reflection geometry [9] mounted on a rotating anode generator. We used a point focus incident beam and monochromatized copper $K_{\bar{z}}$ radiation. The irradiated surface of the sample

Table 1
Unit cell parameters and volume of the HgI_2 films after non-linear least-square unit-cell refinement

Sample	Substrate	N	a (Å)	c (Å)	V (Å^3)	R (%)	Rw(%)
A	$(001)_{KCl}$	13	4.369 (1)	12.437 (1)	237.44	0.02	0.072
B	$(001)_{KCl}$	9	4.368 (1)	12.437 (3)	237.24	0.02	0.077
C	$(001)_{KCl}$	5	4.357 (3)	12.436 (7)	236.02	0.02	0.072
D	$(001)_m$	4	4.372 (4)	12.439 (9)	237.76	0.02	0.093

Notice the relatively low a parameter of film C which exhibits a different texture. N is the number of peaks taken for the refinement.

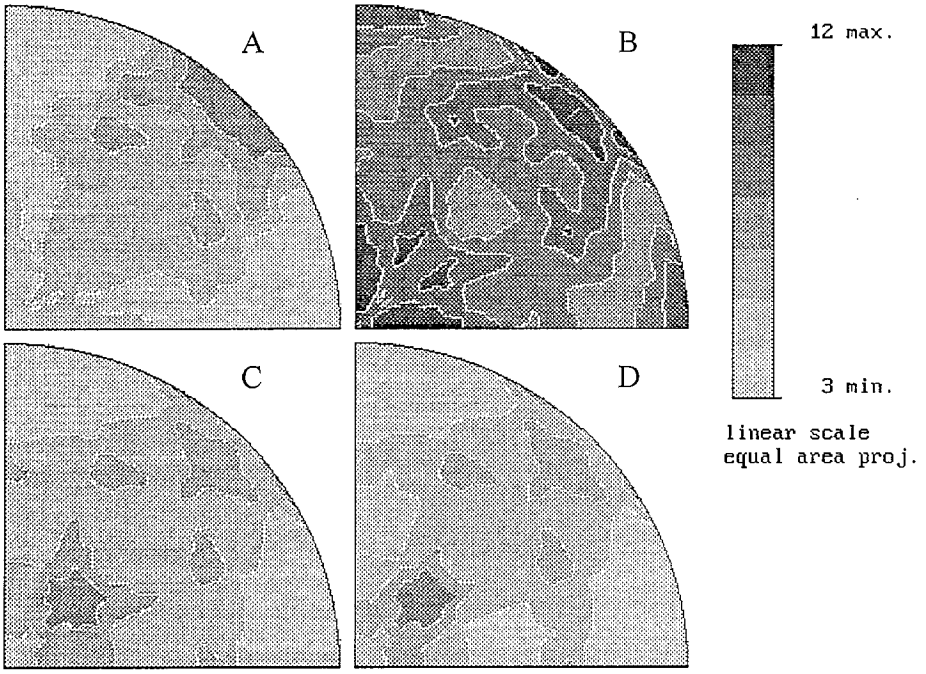

Fig. 1. Inverse pole figures representing the OD space coverage for the analyzed pole figure ranges of Table 2. Scale is in number of path defining each OD cell. Linear scale, equal area projection.

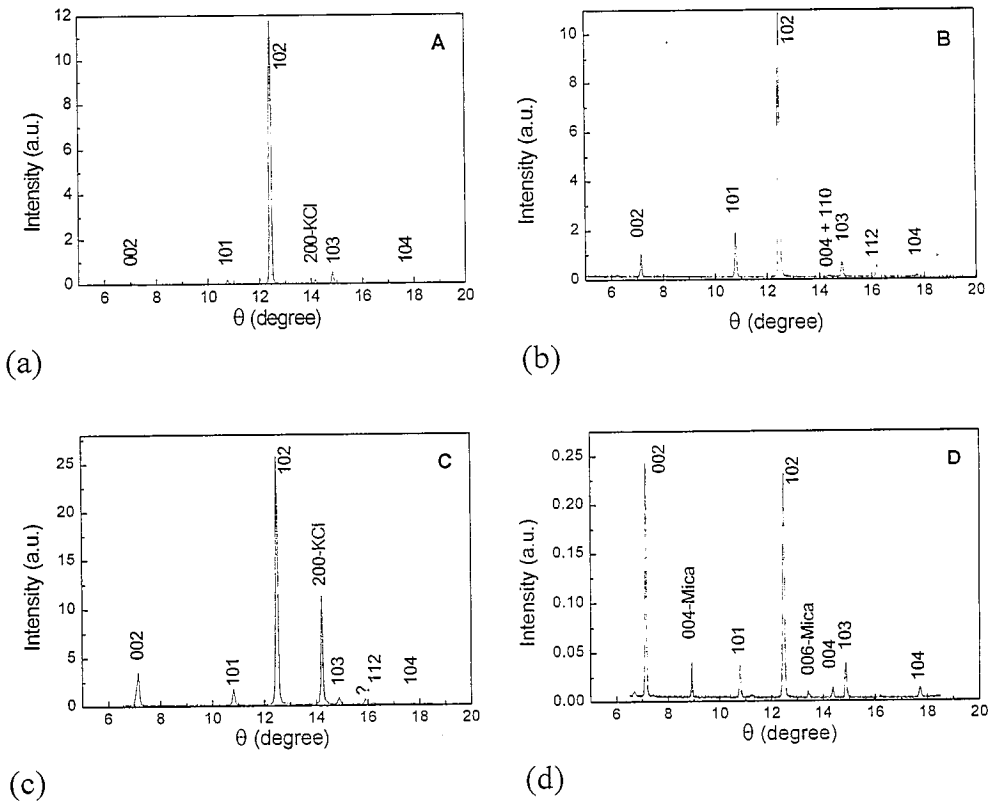

Fig. 2. $\theta-2\theta$ diagrams of the four films A, B, C and D ((a), (b), (c) and (d) respectively). Ratio between diffracted peaks are varying between samples, as an indication of several stabilized textures. Except in film D on muscovite, 102 reflection is stronger than for a random sample.

Table 2
Results of texture refinements

Sample	Pole figures	χ-range (°)	Min OD (m.r.d)	Max OD (m.r.d.)	F^2 (m.r.d.)^2	RP0 (%)	RP1 (%)
A	002, 101, 102	0–60	0	248.2	36.4	43.4	29
B	002, 101, 102, 104, 112	0–60	0	244.5	43.9	23.5	18.9
C	002, 101, 104	0–60	0	51.3	5.6	6.8	6.2
D	002, 101,	0–60	0	62.6	4.8	3.8	3.8
	104	20–60					

Depending on sample, the pole figures were not analyzed in the same ranges. Maxima value and texture index (F^2) indicate strong preferred orientations, while averaged RP factors show the quality of the refinements.

was of the order of several mm^2. The experimental setup gave full widths at half maximum of the $\theta-2\theta$ peaks less than 0.1° in θ in the range of interest. The $\theta-2\theta$ spectra were used to give preliminary information on texture and to determine the peak positions. The peak positions were corrected for systematic shift using the single crystalline substrate reflections, and then used for unit-cell refinement using a non-linear least-square algorithm, CELREF [10]. We then measured pole figures for several peaks of the film. Since we studied different sample shapes and different substrates, the conditions of measurement had to be chosen specifically and are detailed in the text. Pole figures were measured using angle increments in tilt and azimuth rotations (χ and ϕ respectively) as small as $\Delta\chi = \Delta\phi = 0.9°$ or $\Delta\chi = \Delta\phi = 1.8°$, depending on the texture strength, in order to measure the true pole maxima. Measurement ranges were $0 \leq \chi \leq 72°$ and $0 \leq \phi \leq 360°$ for all pole figures. Data were corrected for background, defocusing, absorption and volume variations. Defocusing and background variations with χ were measured on a standard randomly oriented sample, volume and absorption corrections were operated assuming a linear absorption coefficient of 1650 cm^{-1} [11]. Then data were transformed into a $5° \times 5°$ grid by a spline interpolation procedure and analyzed using the texture package BEARTEX [12]. The pole figures were normalized into multiple of random distribution (m.r.d.) and the orientation distribution (OD) calculated using the WIMV refinement algorithm [13] of BEARTEX. From the OD

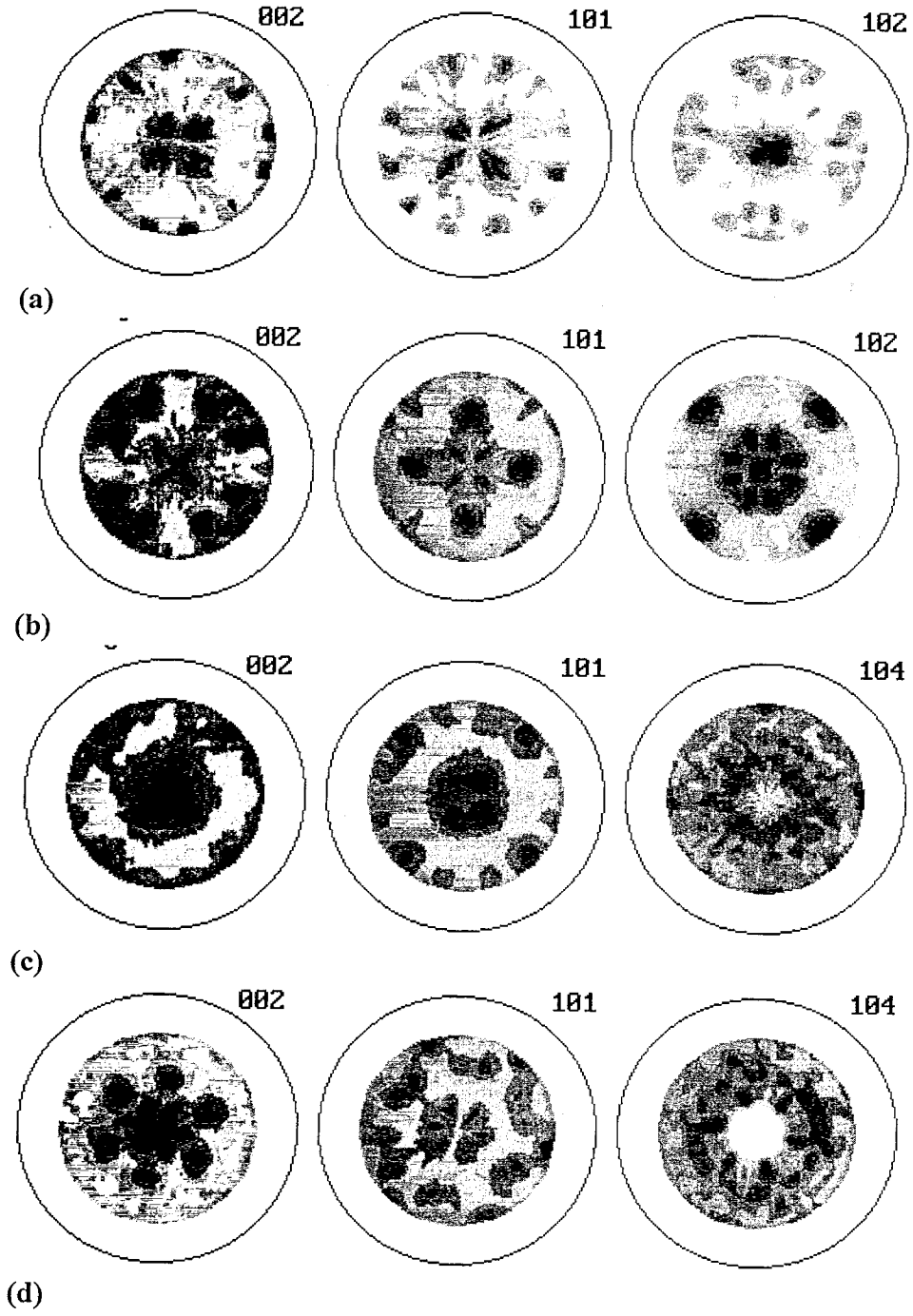

Figure 3

Fig. 3. Measured pole figures of the films A, B, C and D ((a), (b), (c) and (d) respectively) which illustrate the presence of complex textures. These are direct pole figures, hence the intensity scale is not quantitative and not presented. {002}, {101} and {102} pole figures for films A and B, {002}, {101} and {104} for films C and D. Logarithmic intensity scale, equal area projections.

we recalculated pole figures and inverse pole figures. The comparison between experimental (normalized) and recalculated pole figures permitted evaluation of the quality of the OD refinement. Quantitative reliability factors of this refinement are the averaged $\overline{\text{RP0}}$ (for all densities) and $\overline{\text{RP1}}$ (for densities above 1 m.r.d. only) [14]. We also calculated the texture index F^2 which represents the overall texture strength [15].

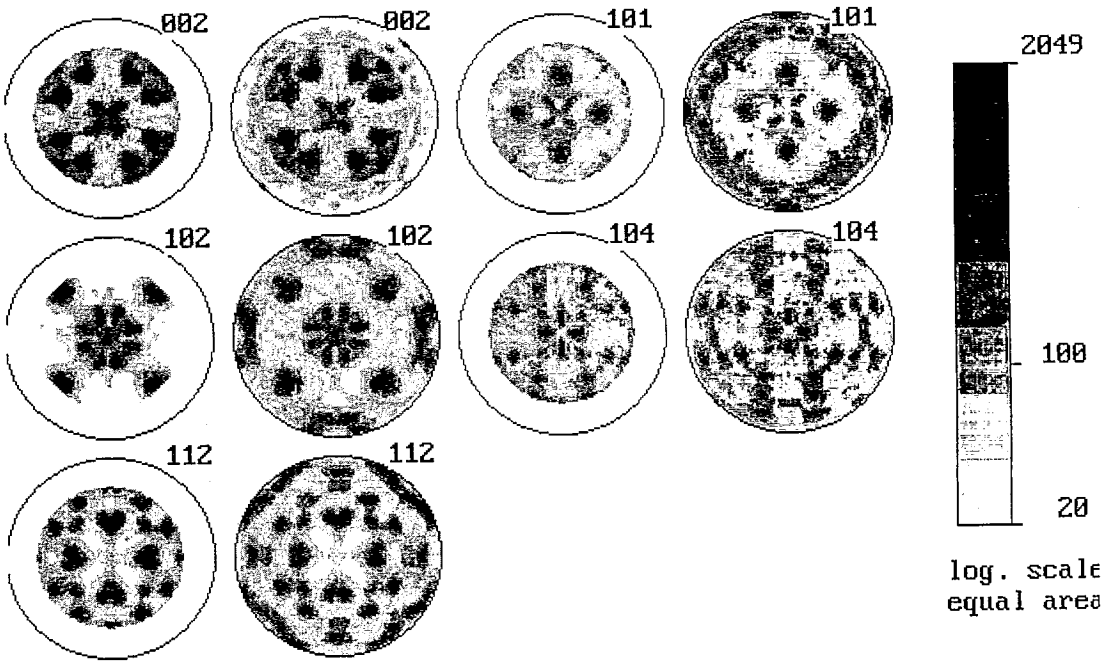

Fig. 4. Normalized-experimental and -recalculated (successively) pole figures of sample B which exemplify the good agreement of the OD refinement. Logarithmic pole density scale in m.r.d., multiplied by 100. Equal area projection.

A {hkl} pole figure represents the distribution of ⟨hkl⟩* reciprocal crystalline directions (normals to the {hkl} planes) in the sample reference frame. the latter is defined by three orthogonal unit vectors, **100**, **010** and **001**, parallel to the main axes of the sample. Here **001** is the normal to the sample plane (pole figures center), **100** and **010** being two perpendicular substrate edges (horizontal and vertical axes of pole figures respectively). Accordingly, a *HKL* inverse pole figure shows which distribution density of every crystal direction is present along a specific *HKL* axis of the sample.

First, we evaluated the orientation space coverage, taking into account the extent of the measured regions of the pole figures (Table 1). This analysis was based on the concept of minimum pole density set, MPDS [16]) which defines as a necessary condition that the pole figure ranges must be sufficient to at least determine every possible single orientation. In the case of discrete methods (WIMV analysis for example) this implies that at least three projection paths from pole figures pass through all OD cells. If we assume that full azimuthal rings have been measured, as in the present work, this condition can be analyzed with inverse pole figures. Results of number of intersections for our films are given in Fig. 1. Values must be at least 3 in all OD cells to completely define the orientation distribution. This condition is satisfied, with values ranging from 3 to 12, even for the sample deposited on muscovite, the orientation distribution being the most accurately determined for sample B.

3. Results and discussion

3.1. θ–2θ diffraction patterns

Fig. 2(a)–(d) show θ–2θ diagrams for the samples A–D respectively, in the 5–20° range. The experimentally analyzed range was extended to 60° in θ, allowing cell refinement on more peaks with a good resolution, as illustrated by the low reliability factors (Table 2). The α form of mercury iodide with tetragonal unit-cell has been successfully synthesized. At this point we can observe that all samples have cell parameters identical to those of bulk α-HgI_2 except sample C for which a unit-cell parameter is smaller, taking into account standard deviations.

We observe strong deviations from random distribution of crystallites, even though all reflections remain, proving the existence of several orientation components. All films deposited on KCl exhibit 102 peak higher than random distribution, sample A showing the highest. The film D on muscovite has a markedly different preferred orientation, with {002} planes parallel to the sample surface. However these primary characteristics of the texture are not quantitative, and might not reveal important components of the texture corresponding to diffracting planes non-parallel to the surface. This is particularly true if a strong texture exists. The possible in-plane orientation is also not accessed in these spectra.

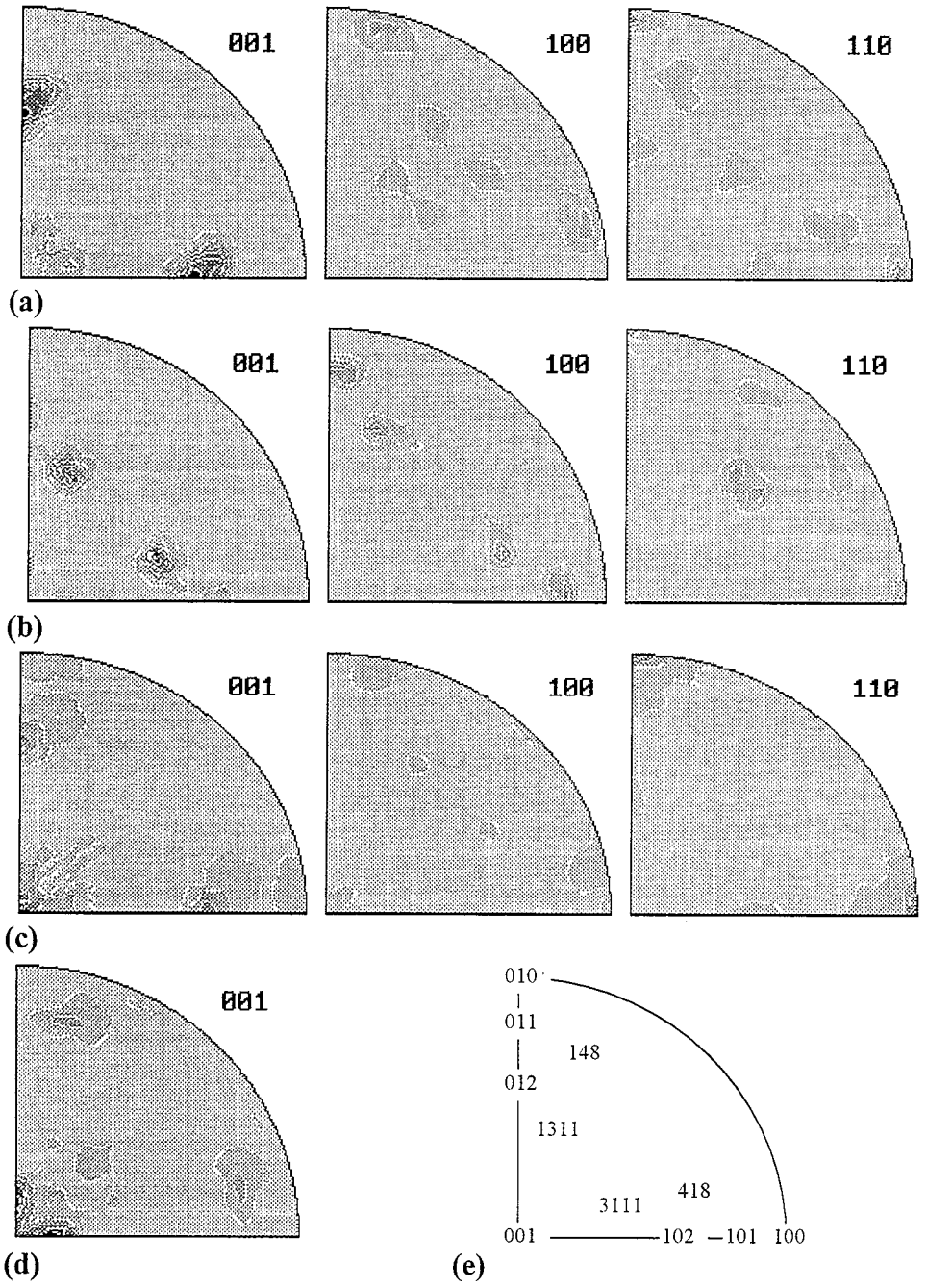

Fig. 5. **001**, **100** and **110** inverse pole figures of (a) samples A, max = 13.3 m.r.d.; (b) sample B, max = 18.3 m.r.d.; (c) sample C, max = 10.3 m.r.d.; (d) 001 inverse pole figure of sample D, max = 9.7 m.r.d.; (e) shows pole indexing. Linear density scale, equal area projection. All minima are 0.

3.2. Pole figures and OD

The pole figures measured on our samples are of complex interpretation. They are relevant of textures developed by several epitaxial relationships. Fig. 3 exemplifies this, for three experimental and normalized pole figures on each sample. As these pole figures are incompletely measured (because of defocusing), it becomes very difficult to visualize epitaxial relationships, only visible at their periphery. This incompleteness is overcome by calculating the OD.

Fig. 4 illustrates results given by the WIMV calculation on sample B. It shows the normalized experimental pole figures, and the recalculated ones from the OD. The principal axes of the sample (*a* axes of KCl) have been aligned parallel and perpendicular to the figure

Table 3
Epitaxial relationship types encountered in our films

Sample	Alignment along the normal to the sample plane	Epitaxial relationship at the substrate interface	Type	Mismatch (%)
A	⟨102⟩*HgI_2//[001]KCl	⟨100⟩HgI_2//[110]KCl	II	1.84
B	⟨3$\underline{1}$1⟩*HgI_2//[001]KCl	⟨101⟩*HgI_2//[100]KCl	III	1.72
		⟨418⟩*HgI_2//[100]KCl		
	⟨102⟩HgI_2//[100]KCl	⟨100⟩HgI_2//[110]KCl	II	1.84
C	⟨001⟩HgI_2//[001]KCl	⟨100⟩HgI_2//[110]KCl	I	1.84
	⟨102⟩*HgI_2//[001]KCl	⟨100⟩HgI_2//[110]KCl	II	1.84
	—	⟨100⟩HgI_2//$\langle 100\rangle^*_m$		15.4
	—	⟨011⟩*HgI_2//$\langle 110\rangle^*_m$	I′	8.1
	—	⟨110⟩*HgI_2//$\langle 010\rangle^*_m$		2.5
D	—	⟨110⟩*HgI_2//$\langle 010\rangle^*_m$	II′	2.5
	—	⟨011⟩*HgI_2//$\langle 110\rangle^*_m$		8.1
	—	⟨100⟩HgI_2//$\langle 010\rangle_m$		3.2
	—	⟨012⟩*HgI_2//$\langle 100\rangle_m$	III′	27.8
	—	⟨100⟩HgI_2//$\langle 100\rangle_m$		15.4
	—	⟨012⟩*HgI_2//$\langle 010\rangle_m$		15.8

Mismatches are calculated respectively to the substrate d-spacing. * stand for reciprocal <hkl> directions (normals to {hkl} planes). For sample D, no direction alignment along the normal is specified since the in-plane epitaxies correspond to irrational hkl along the normal.

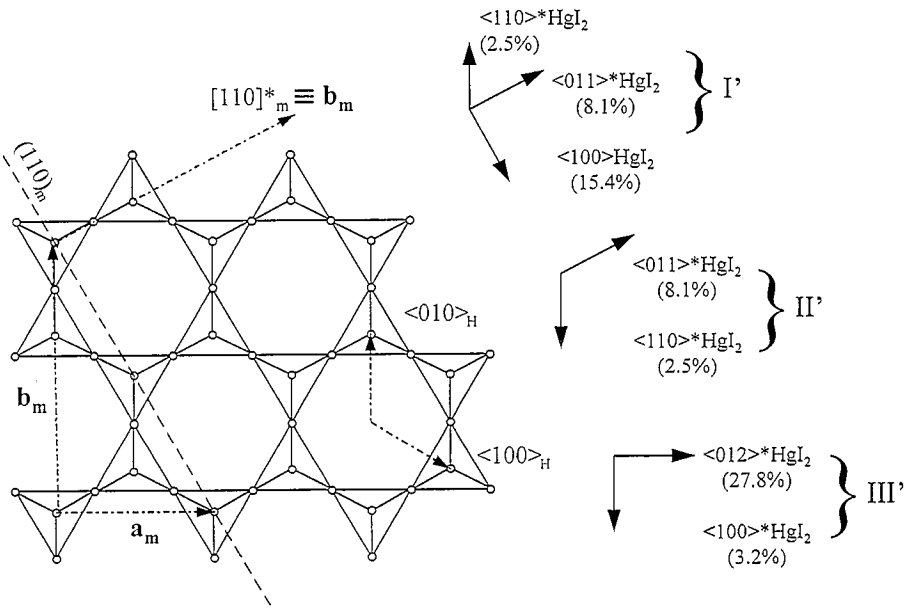

Fig. 6. (a, b) hexagonal-like Si_2O_5 plane of the muscovite structure. Circles represent oxygen atom locations on tetrahedra. The distortion is not shown here for simplicity. a_m and b_m are the monoclinic unit-cell parameter of muscovite. H indices refer to the pseudo-hexagons formed by apical oxygens. One orientation of the three observed orientation types I′, II′ and III′ is indicated. Distance mismatches are given in parentheses.

axes. We observe a very good agreement between experimental and recalculated figures, as illustrated by the RP factors in Table 1 which summarizes the results for all samples. On sample D, the central part of the {104} pole figure has not been used because of the presence of the 008 reflection from the single-crystalline substrate in this region. Both minimum and maximum OD (Table 2) levels are given. They indicate a strong texture for all samples, with minima at 0 and maxima as high as 248 m.r.d. for sample A. The texture index is correlatively very high, particularly for samples A and B. The RP factors are low for all of them, even though only three incomplete pole figures were used for the calculation. In the case of sample A, the RP factors show less satisfying reliability, because of the relatively poor sample geometry, insufficiently regular to provide a constant sample irradiation during the experiment. However since RPs depend on the texture strength, it is normal to have relatively higher values for samples A and B.

One important feature is that we can access the epitaxial relationships with the recalculated figures. For example it is clear that the {101} pole figure exhibits

poles at $\chi = 90°$, indicating that the {101}-HgI_2 crystallographic planes are predominantly perpendicular to the sample plane and stacked along the *a* parameter of the substrate. The geometrical matching between the *d*-spacing of the two structures for this alignment is of only 1.72% (between 202-HgI_2 and 300-KCl). However, one must calculate all the possibilities of alignment (all the pole figures) along the main sample axes, in order to reveal other possible orientation relationships. This can be done more easily by analyzing the inverse pole figures recalculated from the OD.

4. Epitaxial relationships

4.1. Films on KCl

Due to its parameters respecting the relation $c \approx 3a$, the HgI_2 unit-cell can be viewed as pseudo-cubic from the point of view of orientation. It follows that, for example, {114}, {200} and {105} from HgI_2 all match well with the (220) plane spacing, and allow several orientations. As shown in the following, inverse pole figures can separate them.

Fig. 5(a)–(d) represents the **001**, **100** and **110** inverse pole figures of the respective samples. Fig. 5(e) indexes the pole locations. Table 3 summarizes the corresponding heteroepitaxial relationships. Fig. 5(c) clearly shows a {001}HgI_2//(001)KCl preponderant heteroepitaxial relationship (type I) with ⟨100⟩HgI_2 directions aligned on [110]KCl. This heteroepitaxy corresponds to a mismatch of 1.84%. The minor relation encountered in this sample (Type II) corresponds to the principal component of sample A, which exhibits {102}HgI_2 planes parallel to (001)KCl, with the same in-plane relation as type I. Therefore, the same in-plane epitaxial relation can be stabilized with different preferred orientations along the sample normals. Types I and II are competitive. Consequently little changes in preparation conditions can easily modify the proportional ratio between these two types. There are other visible weak poles in the **001** inverse pole figures of sample C. They may be due to other possible distances matching in the plane of the interface which correspond to higher hkl values, considered to be less stable heteroepitaxies.

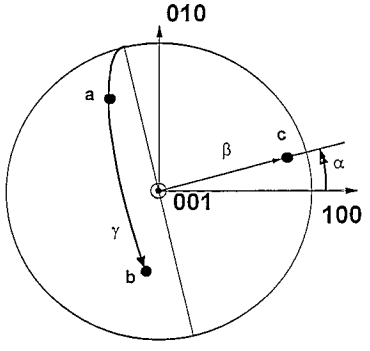

Fig. 7. Definition of the Roe/Matthies Euler angle convention relating crystal (a = [100], b = [010] and c = [001]) and sample (**100**, **010** and **001**) coordinate systems (stereographic projection).

All samples deposited on KCl exhibit the type II component, sample A referencing the strongest, with the highest observed level of OD for this component. For sample B the **100** inverse pole figure shows the alignment with ⟨101⟩*HgI_2//[100]KCl described in the previous paragraph, which presents an equivalent mismatch level as for the other epitaxial types along this direction. This epitaxial orientation is reinforced with the in-plane ⟨418⟩*HgI_2//[100]KCl relation, also visible on the **100** inverse pole figure. Both correspond to an alignment of ⟨3$\underline{1}\underline{1}$⟩*$HgI_2$ (type III) with the sample normal. This is understandable since the angles between {101}, {14$\bar{8}$} and {$\bar{1}$3$\underline{1}\underline{1}$} of HgI_2 (and equivalents by permutation) are almost 90° apart (101^14$\bar{8}$ = 89.8°, 14$\bar{8}$^$\bar{1}$3$\underline{1}\underline{1}$ = 89.56° and 101^$\bar{1}$3$\underline{1}\underline{1}$ = 89.19°. The relatively low angle between {101} and {3$\underline{1}\underline{1}$} explains why the 101 poles of the **100** inverse pole figure of sample B are not perfectly aligned on the edges.

Since the substrate directions involved in the epitaxies have a four-fold symmetry at the interface plane, all these epitaxial relations are also four-fold, each component related to the other by a rotation of 90° around the substrate normal.

4.2. Film on Muscovite

The {002} pole figure of sample D (Fig. 3(d)) indicates two series of six {002} poles located at $\chi = 12°$ and $\chi = 31°$ respectively. Within a series, the poles are related to each other by a rotation of 60° around the sample normal, exhibiting a six-fold symmetrical pattern. This is understandable when looking at the (001) muscovite plane (Fig. 6). The plane is constituted of deformed hexagonal rings (not shown on the figure for simplicity) formed by the Si_2O_5 tetrahedra of the structure. On this figure, a_m and b_m are the monoclinic unit-cell parameters of the muscovite structure, respectively aligned with the $\langle 210 \rangle_H$ and $\langle 010 \rangle_H$ directions of the pseudo-hexagons formed by the apical oxygens of the tetrahedra layer. Using the definition of Fig. 6, the $\langle 110 \rangle_H$ direction is parallel to $[110]^*_m$. Then it becomes evident that each direction which matches along $[110]^*_m$ will also match with all the equivalent directions to $\langle 110 \rangle_H$ and $\langle 100 \rangle_H$, giving rise to the observed six-fold symmetry. b_m then possess six equivalent definitions, one of them represented on Fig. 6. Similarly, all equivalent $\langle 210 \rangle_H$ directions give six possibilities to define a_m.

From the density maxima of the OD we can determine the orientation components corresponding to the

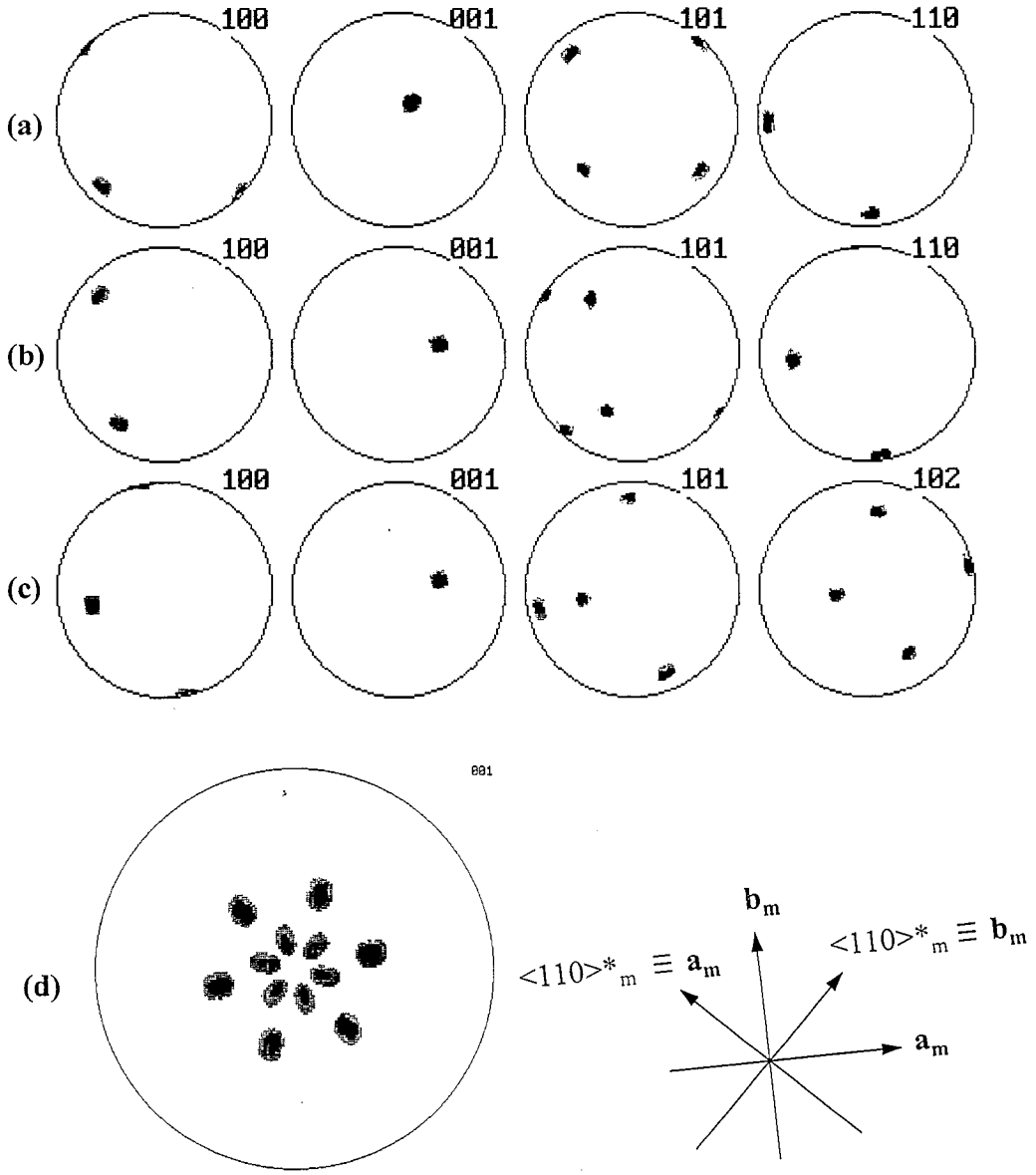

Fig. 8. Theoretical pole figures corresponding to the orientations observed on sample D, respectively for one of the six-fold heteroepitaxies of type I′ (a), II′ (b) and III′ (c). The last {001} pole figure (d) shows the superposition of all these components including the six-fold symmetry. A Gaussian distribution shape of 5° of full width at half maximum was assumed. Types II′ and III′ give superposed {001} poles at $\chi = 32°$. Arrows give the substrate orientation.

observed heteroepitaxies. We chose the Roe/Matthies convention (Fig. 7) for (α, β, γ) Euler angles of the orientation space [17]. Three orientation maxima are observed in the OD. They corresponds to three orientation types. One type (orientation type I′, Table 3) corresponds to $(\alpha, \beta, \gamma) = (48°, 12°, 0)$ for the inner ring of poles of the {002} pole figure (Fig. 3(d)). One orientation of this type is illustrated by the {100}, {001} {101} and {110} theoretical pole figures (Fig. 8(a)), which clearly evidence the in-plane location of the three directions $\langle 100\rangle^*HgI_2$, $\langle 011\rangle^*HgI_2$ and $\langle 110\rangle^*HgI_2$. Main directions of the substrate are indicated for clarity. The three corresponding heteroepitaxial relationship are given in Table 3. From the mismatch value it is expected that the $\langle 100\rangle^*HgI_2$ direction alignment is the less efficient for the stabilization of this relation.

The outer ring of {002} poles of Fig. 3(d) is explained by two other orientation components located at $(\alpha, \beta, \gamma) = (12°, 32°, 40°)$ and $(\alpha, \beta, \gamma) = (12°, 32°, 0)$ (type II′ and III′, illustrated by Fig. 8(b) and (c) respectively). Type II′ is two thirds the distribution density of

type III′, with relatively less favourable lattice plane matching (Table 3). These latter two orientations are superposed on the {001} pole figure at $\chi = 32°$. Type II′ corresponds to the same in-plane orientations as type I′, with the absence of the highest mismatch relation. Type III′ is achieved with higher distance mismatch, and it is not possible to distinguish if $\langle 100 \rangle^* HgI_2$ align with a_m or b_m, both orientation being symmetrically equivalent. Furthermore, the average mismatch factors over the two in-plane relationships is approximately the same for both orientation (Table 3).

Since the three orientation types are related to six-fold substrate directions, the described single orientations are equiprobably retrieved by a rotation of 60° around the normal of the sample. Fig. 8(d) shows the calculated {001} pole figure corresponding to this symmetry for the three types I′, II′ and III′ (compare with Fig. 3(d)). This high number of orientations explains the relatively low texture strength of this film, compared with films deposited on KCl.

As was the case with the samples deposited on KCl substrates, the various heteroepitaxies observed on sample D are stabilized with relatively high distance mismatches. They correspond to orientation types which can be deduced one from the other by simple rotations. This may explain their simultaneous occurrence inside the film.

5. Conclusion

An X-ray diffraction texture investigation of four HgI_2 thin films deposited by sublimation on KCl and Muscovite single crystals has been carried out.

The films were successfully stabilized with cell parameters close to the bulk ones, in the tetragonal form α-HgI_2.

Strong preferred orientations perpendicular to and in the substrate plane are observed whatever the substrate. It was possible to resolve quantitatively all these textures using direct methods for the refinement of the orientation distribution. In-plane alignment of the films is governed by multiple heteroepitaxial relationships, with close distance matching. The different types of textures are deducible by simple rotations one from each other. Consequently, all these epitaxial types are present in comparable ratios in the used deposition condition range. The substrate symmetry at the interface's plane implies that every epitaxial type is four-fold in the case of KCl and six-fold for Muscovite.

Optimization of deposition conditions and physical property measurements are now under investigation.

Acknowledgements

Authors would like to thank J. Coates from University of Washington, for careful reading, improving of English and criticizing of the manuscript.

References

[1] H.R. Wenk, F. Heidelbach, D. Chateigner and F. Zontone, *J. Synchrotron Radiation*, (accepted).
[2] R.B. James, T.E. Schlesinger, P. Siffert and L. Franks, *Mater. Res. Soc. Symp. Proc., 302* (1993) 115.
[3] J.M. Van Scyoc, T.E. Schlesinger, R.B. James, A.Y. Cheng, C. Ortale and L. Van den Berg, *Mater. Res. Soc. Symp. Proc., 302* (1993) 115.
[4] L. Keller, E.X. Wang and A.Y. Cheng, *Mater. Res. Soc. Symp. Proc., 302* (1993) 153.
[5] B. Erler, M. Piechotka and E. Kaldis, *Cryst. Res. Technol., 31* (4) (1996) 479.
[6] National Bureau of Standards, *Mono., 25* (7) (1969) 32.
[7] J. Monier, *Bull. Soc. Franç. Minér. Crist., 57* (1954) 1173.
[8] M. Piechotka and E. Kaldis, *Nucl. Instr. Methods Phys. Res. A, 283* (1989) 111.
[9] L.G. Schulz, *J. Appl. Phys., 20* (1949) 1030.
[10] J. Rodriguez, M. Anne and J. Pannetier, *STRAP*, a System for Time-Resolved Data Analysis (Powder Diffraction Patterns), ILL Int. Rpt., 1992
[11] D. Chateigner, P. Germi and M. Pernet, *J. Appl. Cryst., 25* (1992) 760.
[12] H.R. Wenk, S. Matthies, J. Donovan and D. Chateigner, *J. Appl. Cryst.*, (accepted).
[13] S. Matthies and G.W. Vinel, *Phys. Stat. Sol. B, 112* (1982) K111.
[14] S. Matthies, G.W. Vinel and K. Helming, *Standard Distributions in Texture Analysis*, Akademie-Verlag, Berlin, 1987.
[15] H.J. Bunge, *Texture Analysis in Materials Science*, (PR Morris Trans.), Butterworths, London, 1982.
[16] A. Vadon, Généralisation et optimisation de la méthode vectorielle d'analyse de la texture, *Thesis*, Université de Metz, 1981.
[17] R.J. Roe, *J. Appl. Phys., 36* (1965) 2024.